International Journal of Optics and Applications 2014, 4(4A): 12-24
DOI: 10.5923/s.optics.201401.03

Optical Characterization of "PhoCUS" Refractive Photovoltaic Concentrators

Antonio Parretta[1,2,*], Francesco Aldegheri[1], Carmine Cancro[3], Raffaele Fucci[3], Giorgio Graditi[3], Riccardo Schioppo[4]

[1]Physics Department, University of Ferrara, Ferrara (FE), Italy
[2]ENEA Research Centre "E. Clementel", Via Martiri di Monte Sole, Bologna (BO), Italy
[3]ENEA Research Centre Portici, Via Vecchio Macello, Portici (NA), Italy
[4]ENEA Research Centre "Casaccia", Via Anguillarese, S. Maria di Galeria (RM), Italy

Abstract The light collection properties of PhoCUS C-Module photovoltaic concentration units have been investigated by realizing a rugged "Mock-up" containing the primary refractive optics, a secondary optical element (SOE) and a receiver. To independently investigate the sole collection efficiency of the optical unit, the receiver was realized by an integrating sphere equipped with a photodetector, able to collect, with known efficiency, all the radiation reaching the receiver area. To investigate the optical efficiency of the whole C-Module photovoltaic concentration unit, a concentration silicon cell, previously tested in the PhoCUS C-Modules, was used as receiver. Two methods were applied for the optical measurements, the conventional "direct" method using a parallel beam with solar divergence to irradiate the front side of concentrator, and the "inverse" method using a lambertian source applied in place of the concentrating cell in order to operate the concentrator in the reverse way.

Keywords Solar Concentrators, Photovoltaic Concentrators, Concentration Cells, Refractive Optics, Optical Properties

1. Introduction

The PhoCUS Project (Photovoltaic Concentrators to Utility Scale) started in 2002 at ENEA laboratories in close cooperation with national industrial operators, to develop a low cost concentrator technology [1-3]. At that time, the high efficiency c-Si solar cells technology seemed the most suitable to be investigated mainly due to its robustness, market availability and technical advantages associated with its relatively low cost. The chose route map of the project was to work with a concentration ratio of around 200 X, based on a conventional frontal grid c-Si cell architecture. The ENEA technology for large area two side contacted c-Si solar cells was then improved in Portici Research Centre for this application to achieve the required performance under the expected concentration. Primary optics were manufactured as PMMA refractive elements by injection molding. A secondary optical element was included to minimize the optical losses due to module assembly and tracking inaccuracies. In this paper, the light collection properties of PhoCUS C-Module concentration units are investigated by realizing a rugged "Mock-up" containing the primary refractive optics, a secondary optical element (SOE) and a receiver. The optical characterization was carried out following two methods; the first is a traditional method largely used in the photovoltaic laboratories, which uses a parallel beam with solar divergence to irradiate the front side of concentrator, from this the name "direct" associated to this method. The second method [4] uses a lambertian source applied to the exit aperture in place of the concentrating cell in order to irradiate the concentrator in the reverse way; from this the name "inverse" associated to this method. More details about the difference between the two methods, their advantages and disadvantages, will be reported in a forthcoming section.

* Corresponding author:
aparretta@alice.it (Antonio Parretta)
Published online at http://journal.sapub.org/optics

2. The "PhoCUS" CPV System

The standard solar PV system is assembled on a single alt-azimuthal solar tracker with a 5 kW nominal power, 32 m^2 area, and is realized by 51 C-modules of 0.65 m^2 area and 105 W power each (see Fig. 1).

The type of motion is tracking and pointing (closed loop); the tracking speed is 15°/h; the pointing velocity is 3°/min; the accuracy is ± 0.2°; the trajectory correction is closed loop and open loop in case of failure; the tracker operates up to a wind velocity of 90 km/h.

The photo of the PhoCUS solar tracker during the assembly process is shown in Fig. 2. The modules are

interconnected in 3 parallel strings of 17 series connected C-modules (17s-3p) and the power conditioning unit is realized by an inverter for 4.6 kVA.

Figure 1. Standard solar PhoCUS CPV system (5 kW nominal power) installed at ENEA-Portici Laboratories (Portici, NA, Italy)

Figure 2. The PhoCUS solar tracker during the assembly process (ENEA - Galileo Avionica - ATEC Robotics collaboration). The tracking plan is of 32 m^2

The pilot plant, of 25 kW nominal power, is realized by 5 standard units, with distributed electrical scheme (ring at low voltage); the geometric scheme is symmetric square; the filling factor of ground is GER 0.15-0.25 and the shadowing loss is <3%. The location of the pilot plant is at Area Sperimentale di Monte Aquilone, Manfredonia (FG), South Italy. The pointing precision of the "PhoCUS" solar tracker is reported in Table 1.

Table 1. Pointing precision of the "PhoCUS" solar tracker

Wind velocity (km/h)	Angular precision (°)
V < 40	± 0.2
40 < V < 60	< ± 0.3
60 < V < 90	< ± 0.7
> 90	Stove position

Further improvements have been pursued to realize a lower cost solar tracker. Fig. 3 shows the new low-cost solar tracker installed at the site of ENEA-Manfredonia.

The new solar tracker has the following properties: i) plane realized with box beams instead of welded lattice beams; ii) area of the heliostat of 35 m^2; iii) replacement of planetary gearboxes with chain drive; iv) maximum precision of ± 0.4° at wind velocity < 40 km/h; v) dedicated electronic control, developed by ENEA. ENEA has developed laboratories for the characterization and qualification of the components used on the CPV systems [5]. Fig. 4 shows, as an example, one of these laboratories in operation at Manfredonia site.

Figure 3. The new PhoCUS CPV system realized with the low-cost solar tracker, installed at ENEA-Manfredonia Laboratories

Figure 4. Laboratory for the test of small and medium size inverters in the site of ENEA-Manfredonia Laboratories

For the realization of the first PhoCUS C-Module prototype, Sun Power commercial back contact, high efficiency, FZ monocrystalline HECO252 silicon solar cells were selected (see Fig. 5a); with an active area of 11 x 11 mm^2 these cells are optimised for concentration ratios from 100 to 400 suns (10 W/cm^2 to 40 W/cm^2) and for AM1.5D spectrum.

The conversion efficiency at AM1.5D and 25°C is 25% at 100 suns (P = 3W) and 23.5% at 250 suns (P = 7.1W). The cell is assembled on a AlN substrate and is provided on top with a thin glass sheet doped with 5% Cerium.

The first c-Si solar cells realized in our laboratory showed efficiencies of about 20.0% at 1 sun and 22.0% in the 20-40

suns range (see Fig. 5b). The efficiency remains higher than 20.0% up to 100 sun [6]. Further improvements were then achieved for the c-Si solar cell technology realizing a new grid (see Fig. 6), a new ARC and dimensions optimized for the different concentration levels were adopted. The new cell of 0.64 cm^2 area showed an efficiency > 22% at 100 suns, whereas the new cell of 1.21 cm^2 area showed an efficiency > 20% at 200 suns (see Fig. 7).

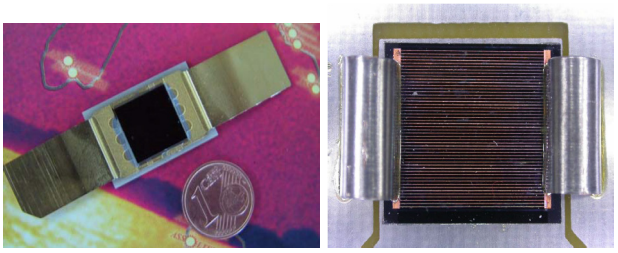

a) b)

Figure 5. a) The HECO252 SunPower Corporation (USA) back-contact high efficiency silicon solar cell used for the first tests of the "PhoCUS" CPV system. b) The ENEA high-efficiency c-Si solar cell with linear grid

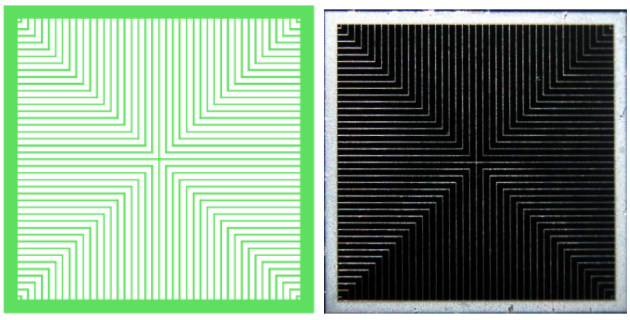

a) b)

Figure 6. a) The square-grid pattern adopted for the new c-Si solar cell. b) The new square-grid c-Si solar cell

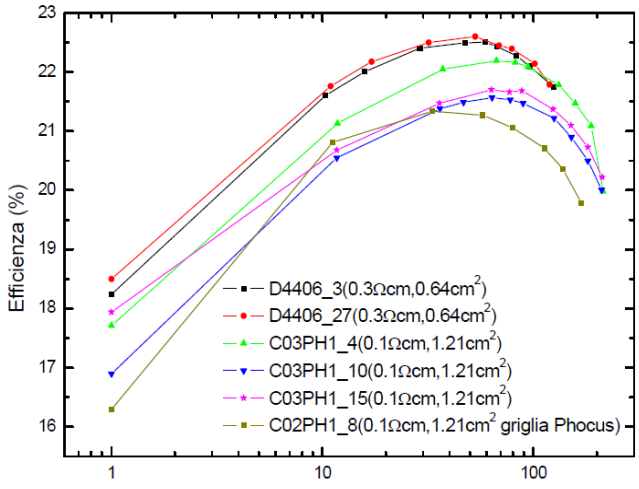

Figure 7. Conversion efficiency curves of the innovative c-Si solar cells developed at ENEA

3. Experimental

The PhoCUS C-module (see Fig. 8) has been realized by the following main components: i) plastic housing; ii) front window consisting of the optical parquet; iii) a secondary optics element (SOE); iv) the solar cells; v) heat sinks for passive cooling of solar cells. Its properties are: dimension of 1 x 0.68m^2, 24 (6x4) series connected solar cells, Voc = 19V, Isc=6.6A, Ppeak=103W. The 200X geometric concentration level has been realized by means of plastic refractive optics, in collaboration with Borromini Srl.

These optics have been assembled as an array of 24 (6x4) lenses. Two main long term targets, in terms of efficiency and economical aspects, were set. The strategy involved the use of plastic structured optics for concentrating solar beams on the PV receiver of the system, instead of more traditional materials like glass and quartz.

Figure 8. Photo of the PhoCUS C-Module, realized by a joint venture ENEA – EniTecnologie

The injection molding technology was preferred for its large throughput and the very low unit cost and PMMA (polymethylmethacrylate) was selected for its superior performance to UV aging. Two types of lenses were used (see Figs. 9 and 10). The first is a "prismatic" lens made of an array of square refractive prisms (see Figs. 9a and 10a): the prism area was 7.8x7.8 mm^2 in the central region, and 3,9x3,9 mm^2 in the periphery [7]. In a second stage another optical device named "hybrid" lens was realized by removing the small peripheral prisms and replacing them by Fresnel grooves (see Figs. 9b and 10b) [8].

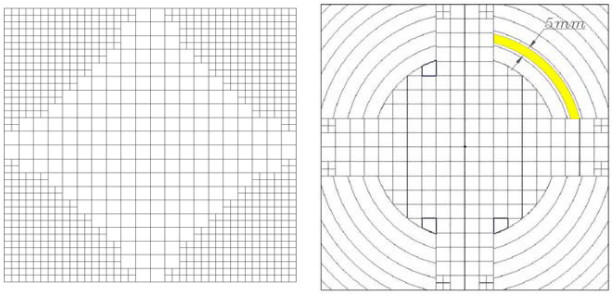

a) b)

Figure 9. Prismatic (a) and the hybrid (b) lens optical models

An optical efficiency of 80% was measured for the prismatic lens and 82% for the hybrid lens, in both cases without the use of an ARC coating. The prismatic lens produces an irradiance map rather uniform for a large portion

of the cell, but also undesired optical losses at the small peripheral prisms mainly due to scattering at the rounded edges and grooves. These drawbacks were removed by the design of the second "hybrid" lens. The lens area is, in both cases, of 243 cm^2 (15.6x15.6 cm).

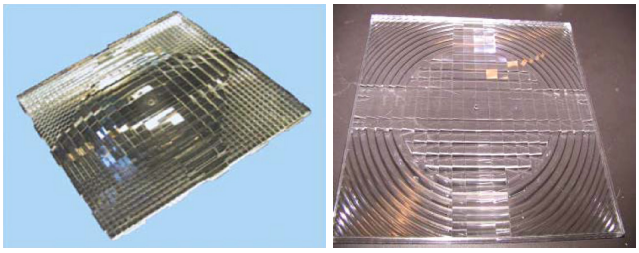

a) b)

Figure 10. Photos of the prismatic (a) and the hybrid (b) lens

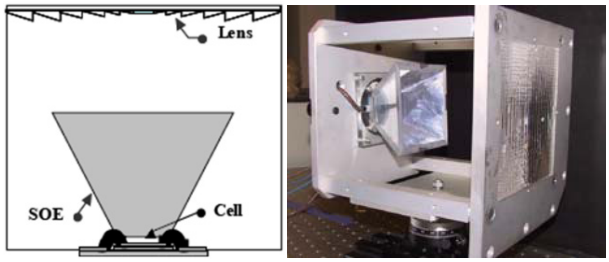

a) b)

Figure 11. Schematic (a) and photo (b) of the Mock-up assembly comprising the primary lens, the secondary optics (SOE) and the solar cell

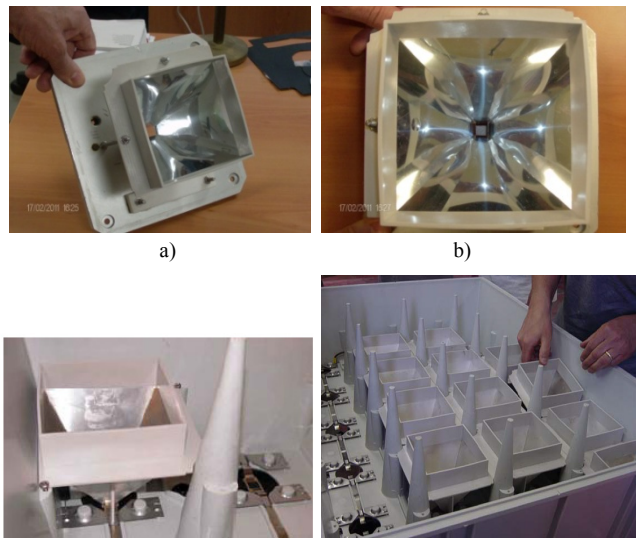

a) b)

c) d)

Figure 12. The secondary optics element (SOE) (a, b) and its view when assembled in the plastic housing of the C-Module (c, d)

The C-Module concentration unit has been studied by indoor measurements performed on a rugged "Mock-up" realized as depicted in Fig. 11. The SOE used for the PhoCUS C-module (see Fig. 12) has the shape of a truncated inverted pyramid with tilt angle of 63° [9, 10]. This value assures the better optical condition in terms of solar light collection for tracking angle inaccuracy (misalignments) of ±1°. The down slit opening is positioned on the upper face of the cell. The SOE used in the Mock-up was made of a transparent polycarbonate substrate coated by a first layer of evaporated aluminium of 2μm thickness covered by a reflecting polymeric film (VM2002 Radiant Mirror Film of 3M). This combination of materials assures a >95% reflectivity in the spectral range of the Silicon cell (see Fig. 13).

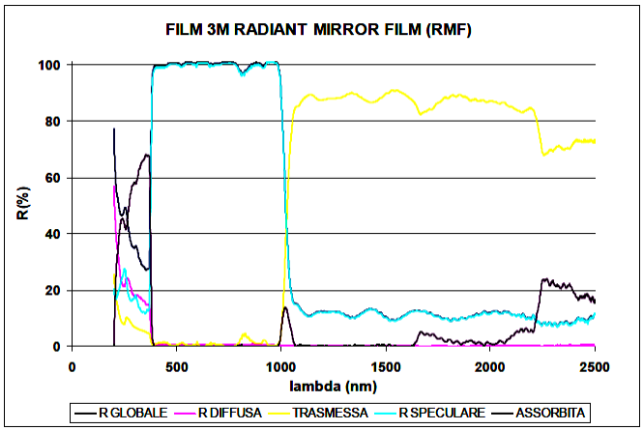

Figure 13. Optical properties of the 3M VM2002 polimeric film (the azur curve corresponds to the specular reflectance)

4. Characterization Methods

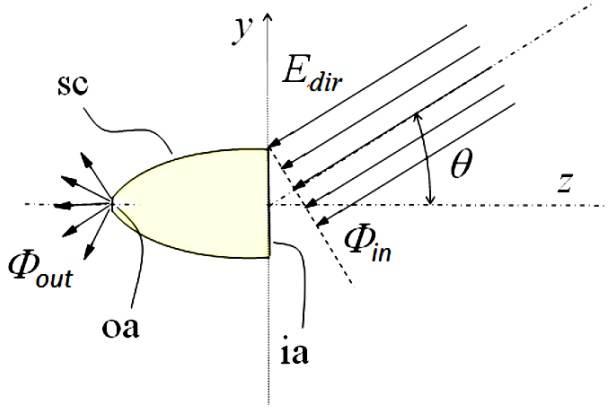

Figure 14. Basic scheme of the "direct" method

The light collection properties of the C-Module concentrating unit were studied in two ways: by the conventional "direct" method and by the "inverse" method [4, 11-23]. In the "direct" method (see the basic scheme in Fig. 14) a parallel beam, simulating the direct component of solar light, is used to irradiate the solar concentrator (sc) oriented at different angles in order to obtain the optical efficiency resolved in angle (optical transmission curve). The optical efficiency of concentrator is obtained by measures of the input flux $\Phi_{in}(\theta,\varphi)$ and of the output flux $\Phi_{out}(\theta,\varphi)$, functions of the polar and azimuthal angles of the collimated input beam:

$$\eta_{dir}(\theta,\varphi)=\frac{\Phi_{out}(\theta,\varphi)}{\Phi_{in}(\theta,\varphi)}=\eta_{dir}(0)\cdot\eta_{dir}^{rel}(\theta,\varphi) \quad (1)$$

The typical experimental set-up of the direct method is schematically reported in Fig. 15a. The lamp (ls) irradiates the integrating sphere (is1) which acts as a lambertian source at its exit aperture. The light emerging from the sphere is collected by the parabolic mirror (pm1), placed slightly off-axis and at a distance from the sphere equal to its focal length *f*.

The mirror (pm1) produces a quasi-parallel beam whose angular divergence can be controlled by varying the diameter of the exit window of sphere. The parallel beam is finally used to irradiate the Mock-up. The light at the exit aperture of concentrator (sc) is collected by the second sphere (is2) (see also Fig. 15b) and its flux measured through photodetector (pd); in alternative, it can be directly collected by the SunPower cell and the flux measured by its photocurrent.

Fig. 15 shows only the measure of the output flux; to measure the input flux, it is necessary to change the experimental configuration. The concentrator must be removed and the parallel beam directed to a second parabolic mirror, which concentrates the light directly into the second sphere (is2) thereby measuring the input flux, apart a small optical loss, known, due to reflectance of the mirror [21].

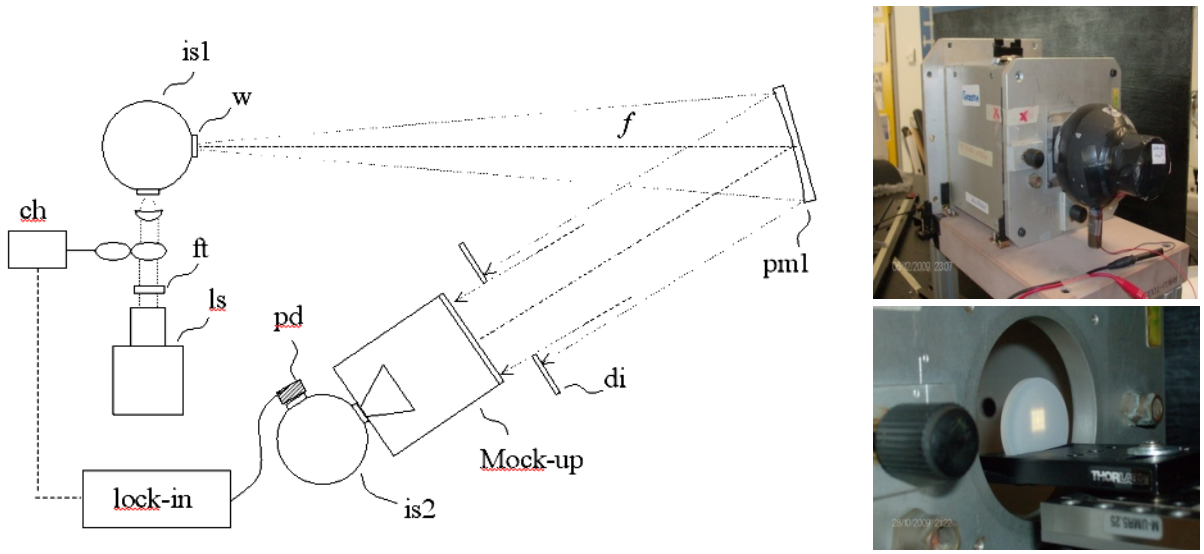

Figure 15. Experimental set-up of the "direct" method applied to the PhoCUS concentrator (a); in (b) it is shown the photo of the receiver station (top) and the square shaped image of the focus produced by the prismatic lens (bottom)

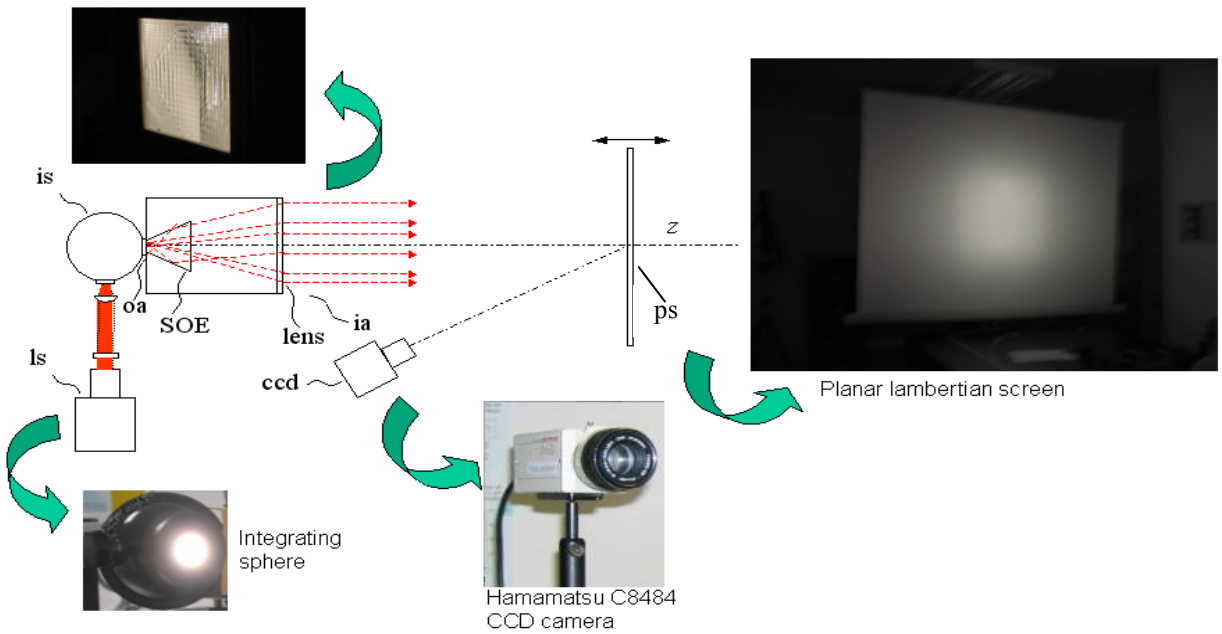

Figure 16. Experimental set-up of the "inverse" method applied to the PhoCUS concentrator

In this way we are able to use two types of receivers in the "direct" method: an integrating sphere or a solar cell. When we match the Mock-up to the integrating sphere provided with a photodetector inside, due to its ideal collecting properties, we are able to measure the light incident on the receiver without losses for reflection at the solar cell surface; we investigate in this way the optical properties of the concentrating unit alone, excluding the photovoltaic receiver. In contrast, by replacing the integrating sphere with the solar cell and by measuring its photocurrent, we investigate the collection properties of the whole, real concentrating unit. By comparing the two measurements, we are finally able to know the optical loss introduced by the solar cell by reflection or scattering of light. The lambertian source of Fig. 15a can be also realized by a white LED source, which shows good lambertian properties in the limited solid angle intercepted by (pm1) mirror.

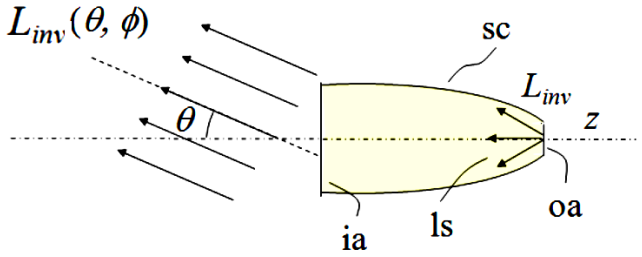

Figure 17. Basic scheme of the "inverse" method

The basic scheme of "inverse" method is shown in Fig. 17. The solar concentrator (sc) is irradiated in a reverse way by a lambertian source of radiance L_{inv}, then it emits light in the reverse direction, with radiance $L_{inv}(\theta,\varphi)$. The inverse method consists in measuring this radiance, because it is related to the optical efficiency of the concentrator. The complete experimental set-up of inverse method is schematically shown in Fig. 16. The integrating sphere (is) is irradiated by the light source (ls) and a lambertian light is produced at the output window (oa) which irradiates the concentrator in the inverse mode. The light is then projected outside the concentrator towards a far planar screen (ps). Fig. 18 shows the input aperture of the PhoCUS concentrator as it appears in the dark when irradiated in the inverse way, and the corresponding image produced on the planar screen. In Fig. 18b some black dots are visible on the light image, which are used to calibrate the distances from the points on the screen, and then to obtain the angle θ to assign to each point P (see also Figs. 17 and 19). The intensity of light on the screen (irradiance) is measured by the CCD, elaborated at a computer and finally transformed in the inverse radiance $L_{inv}(\theta,\varphi)$. The angular distribution of $L_{inv}(\theta,\varphi)$ is obtained by normalizing it at the 0° value. The normalized, or relative, radiance is indicated as $L_{inv}^{rel}(\theta,\varphi)$ and corresponds to the normalized, or relative, efficiency $\eta_{dir}^{rel}(\theta,\varphi)$ obtained with the direct method [4, 13, 14, 17, 19].

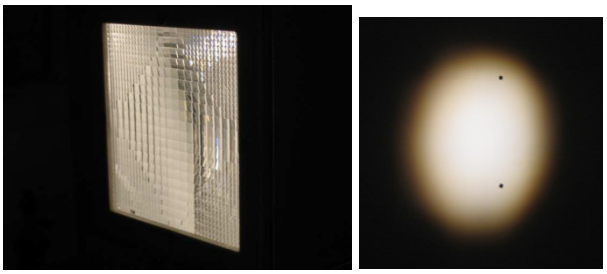

a) b)

Figure 18. In (a) the input aperture of the PhoCUS concentrator as it appears in the dark when irradiated in the inverse way; in (b) it is shown the corresponding image produced on the planar screen

The steps to find the normalized radiance are described below. First of all, the application of the inverse method requires that the following conditions be fulfilled: i) the screen (ps) must be placed as far as possible from the concentrator; ii) it must be an ideal (or quasi-ideal) lambertian diffuser, which means that its total reflectance does not depend on the angle of incidence of the beam, and that light is diffused at constant radiance; iii) the CCD must be aligned along the optical axis of concentrator, otherwise a complex procedure must be adopted to correct the perspective [24]. Point i) requires that the screen (ps) be kept at a distance $d >> D$, diameter of the input aperture. In case of a concentrator with non circular aperture, L can be substituted by $\sqrt{A_{in}}$, with A_{in} area of the input aperture. The angular resolution of the intensity on the screen, in fact, increases at increasing the distance of the screen from the concentrator as it is illustrated in Fig. 19, and is equal to:

$$\Delta\theta \approx \frac{L\cos^2\theta}{2d} \approx \frac{L}{2d} \tag{2}$$

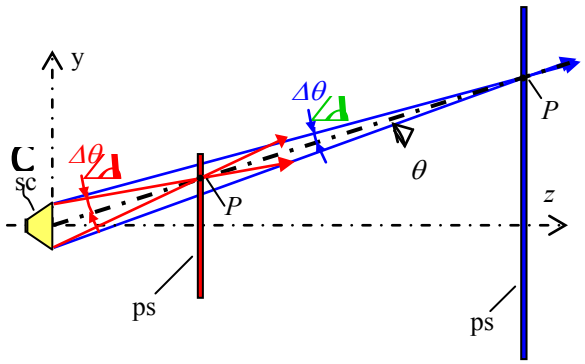

Figure 19. The angular resolution $\Delta\theta$ on the point P of the screen improves increasing the distance of the screen from the concentrator

If the above conditions are fulfilled, the CCD image can be elaborated in the following way. The light intensity profile of the CCD image, $I_{CCD}(\theta,\varphi)$, is first normalized to the $\theta = 0°$ value, obtaining $I_{CCD}^{rel}(\theta,\varphi)$, where θ is the polar angle and φ the azimuthal angle of light emission; the intensity $I_{CCD}^{rel}(\theta,\varphi)$ is then multiplied by the factor $(\cos\theta)^{-8}$ to obtain the normalized radiance $L_{inv}^{rel}(\theta,\varphi)$.

A different elaboration applies when simulation programs are used to calculate the normalized radiance; in this case, in fact, the screen is made of an ideal absorber and the normalized radiance is obtained from the normalized irradiance on the screen by multiplication by the factor $(\cos\theta)^{-4}$. The details of this calculation procedure are reported in Appendix.

As the final step, the (adimensional) normalized inverse radiance $L_{inv}^{rel}(\theta,\varphi)$ of the concentrator operating in the reverse way, is set equal to the (adimensional) relative optical efficiency $\eta_{dir}^{rel}(\theta,\varphi)$, measured when applying the direct method (see Figs. 14, 15).

The inverse method allows to measure in a simple way also the absolute on-axis (0° incidence) optical efficiency of the Mock-up, $\eta_{dir}(0)$. Whereas this measure requires the use of a second parabolic mirror with the direct method, as it has been already discussed [21], the inverse method gives the same result in a direct and easy way (see Fig. 20 and the theory in ref. [14])

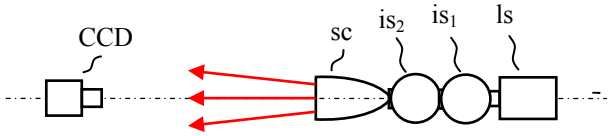

Figure 20. Basic scheme of the experimental set-up to use for determining the on-axis optical efficiency of the solar concentrator (sc). The CCD camera is oriented towards the concentrator irradiated in inverse mode, and the image of the input aperture is recorded

It is sufficient, in fact, to orient the CCD towards the concentrator, aligned with the optical axis, and to take two images: one of the full input aperture with the lens, and the other of the output aperture after removing the lens. In the first image it is taken the mean radiance of the lens, $\overline{L}_C(0)$; in the second image it is taken the mean radiance of the sphere cavity L_S, corresponding to the lambertian source. The ratio between these two quantities gives the absolute on-axis optical efficiency of concentrator $\eta_{dir}(0)$ and, from Eq. (1), the absolute angle-resolved optical efficiency:

$$\eta_{dir}(0) = \frac{\overline{L}_C(0)}{L_S} \tag{3}$$

5. Results

5.1. Optical Simulations

The focalization properties of the two lenses (prismatic and hybrid) without SOE were simulated by TracePro with 100k rays. Fig. 21 shows the images produced at the focal distance of the two lenses. Only the prismatic lens gives a uniform distribution of flux on the focal plane. To obtain a good flux distribution with both lenses the distance lens-receiver was fixed at a constant value of 23 cm, greater than the focal length.

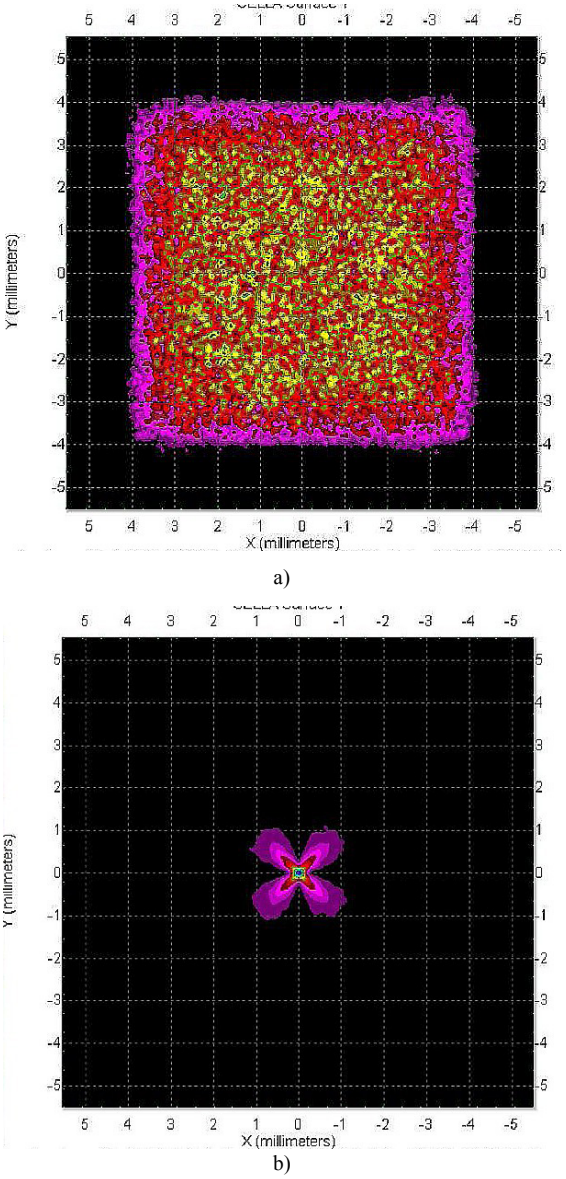

Figure 21. Image of the focused beam at the focal distance of the prismatic (a) and hybrid (b) lens, taken with an incident beam parallel to the optical axis

The simulations of the inverse method required 2M rays and were carried out at a concentrator-screen distance of 3.8 m, the same used in the experimental measurements. Fig. 22 compares the "relative" optical efficiency of the two lenses, obtained by applying the direct and inverse methods. The curves refer to an azimuthal angle of 0° or 90°, that is to an incidence plane of a direct beam parallel to one side of the square lenses.

First of all we observe that the curves of Fig. 22 are typical of an "imaging" concentrator, with a monotonic decrease of efficiency, in contrast to "nonimaging" concentrators, characterized by a plateau followed by a rapid decrease in correspondence of the acceptance angle (angle at 50% of maximum efficiency. The acceptance angle is 1.5÷2.0° at 50% relative efficiency and ~0.5° at 90% relative efficiency. We observe also that i) the two lenses have similar curves for the same method; ii) each method gives similar curves for the

two lenses. The inverse curves gives a slightly larger acceptance angle due to the non-zero angular resolution, as from Eq. (2). In the actual case, with $d = 380$ cm and $L = 15.6$ cm, we have $\Delta\theta$ of the order of 1.2°. The noise in the inverse curves is due to the limited number of rays used in the simulations. The inverse method has been also applied to simulate the concentrator with the SOE and the relative efficiency curves for the two lenses are shown in Fig. 23.

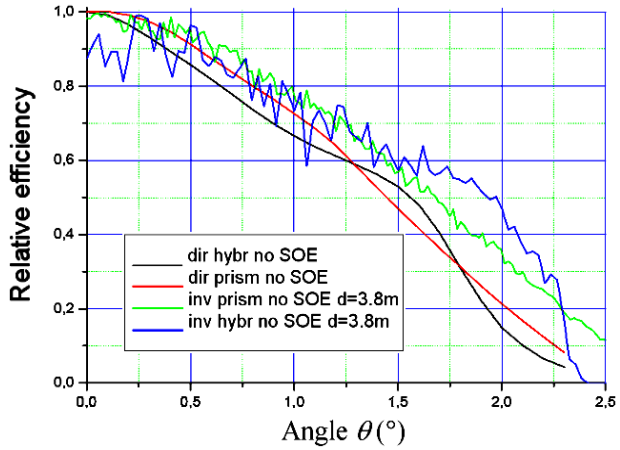

Figure 22. "Relative" optical efficiency of the prismatic and hybrid lenses obtained by applying the direct and the inverse methods

The effect of SOE is to increase the acceptance angle (now of ~2.4° at 50% relative efficiency and ~1° at 90% relative efficiency) for both lenses, as expected, and to equalize the two curves.

The chromatic aberration introduced by the prismatic lens has been studied by simulating, with direct method, the image produced on the receiver by blue light ($\lambda = 450$ nm) and red light ($\lambda = 650$ nm). The results are visible in Fig. 24. Being the receiver behind the focal plane, the short wavelengths are more expanded on the receiver surface.

A summary of the acceptance angles measured by simulations on the two lenses is reported in Tab. 1. The acceptance angles are distinguished between those measured at 50% efficiency and those measured at 90% of 0° efficiency.

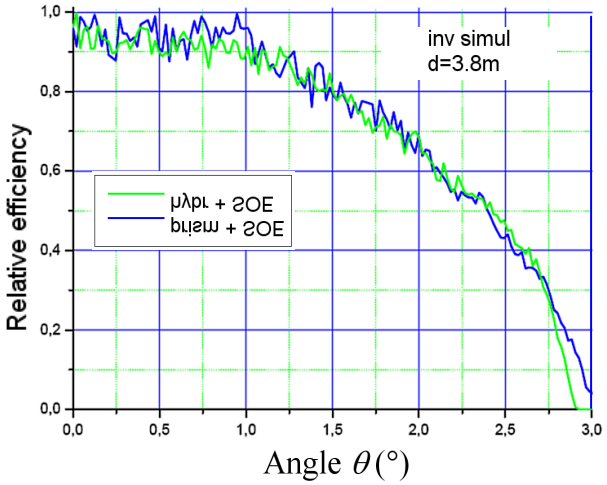

Figure 23. Optical efficiency of the lenses (prismatic and hybrid) obtained by applying the inverse method

Table 1. Summary of simulated acceptance angles

Met.	Lens	Prismatic		Hybrid	
	SOE	50%	90%	50%	90%
Dir.	No	1.4	0.5	1.5	0.4
	Yes	-	-	-	-
Inv.	No	1.7	0.6	1.9	0.5
	Yes	2.4	1.1	2.4	1.1

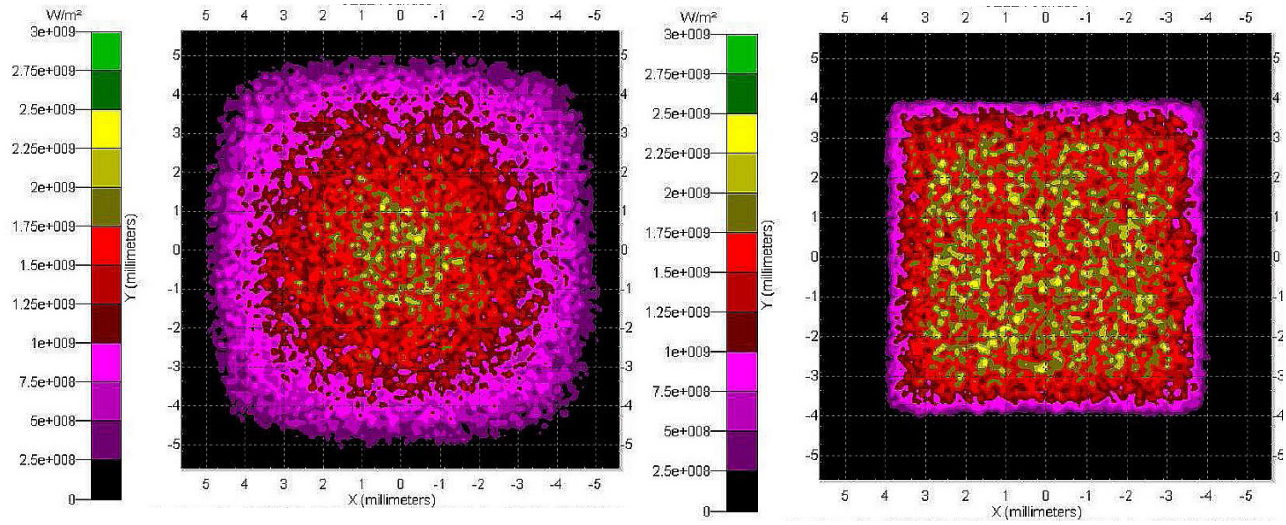

a) b)

Figure 24. Images of the flux on the receiver plane, at 23 cm from the lens, due to $\lambda = 450$nm light (a) and $\lambda = 650$nm light (b)

5.2. Experimental Measurements

The results of the experimental direct method applied to the prismatic lens without SOE, having an integrating sphere or a solar cell as receiver, are shown in Fig. 25, compared to the simulated results.

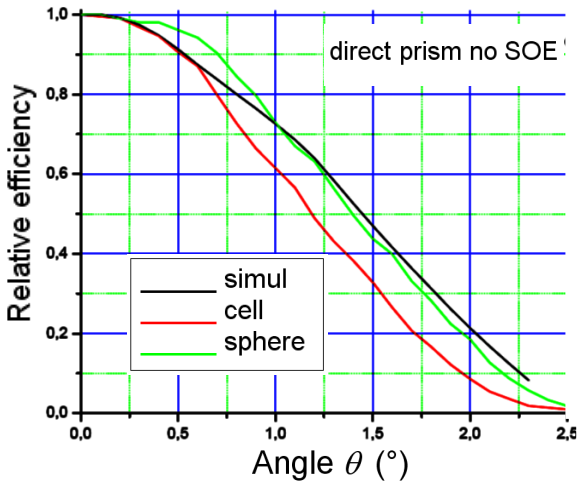

Figure 25. Comparison between the experimental and simulated direct efficiency curves of the prismatic lens without SOE

Fig. 25 shows that coupling the concentrator to the integrating sphere gives the optical properties of the concentrator alone, as obtained by simulations, confirming that the integrating sphere behaves as an ideal receiver. The use of the solar cell, on the contrary, gives a thinner curve, showing that the solar cell is not able to collect with the same efficiency all the incident light, particularly that incident at input at higher angles. The knowledge of difference between the sphere and the cell curve is important to establish how much the cell could be optimized to improve its light collection. Similar results were obtained with the hybrid lens, as shown in Fig. 26.

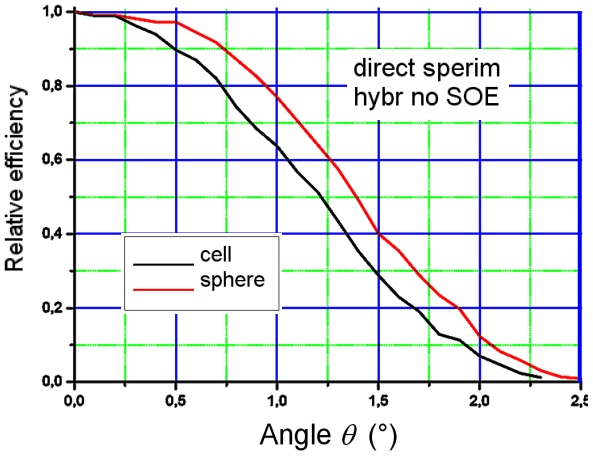

Figure 26. Experimental direct efficiency curves of the hybrid lens without SOE, obtained by using a sphere or a solar cell as receiver

The results of the experimental direct method applied to both lenses in presence of the secondary element SOE, having the integrating sphere or the solar cell as receiver, are shown in Fig. 27. We note now that the prismatic lens + SOE system and the hybrid lens + SOE system have a very similar behaviour; the efficiency curves for the two lenses in fact coincide when the same receiver is used. These results, which were anticipated by the simulations with the inverse method (see Fig. 23), show that the presence of SOE removes the differences in behaviour between the two lenses.

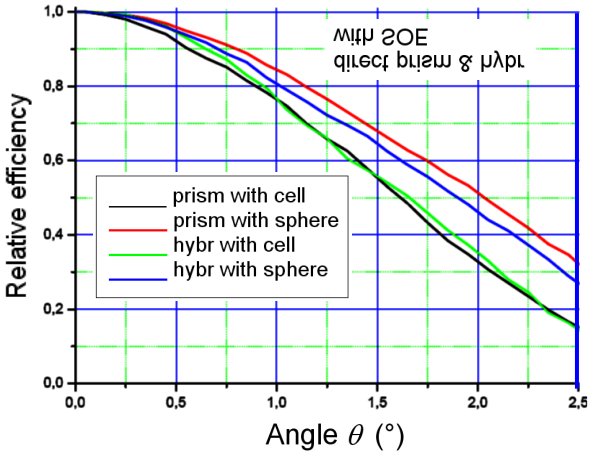

Figure 27. Experimental efficiency curves of the two lenses obtained with the direct method adding the secondary SOE to the concentrator

The adding of SOE to the concentrator has the effect to increase the optical efficiency particularly at high angles, that is to increase the acceptance angle at 50% efficiency; being negligible the increase of acceptance angle at 90% efficiency.

A summary of the experimental acceptance angles, measured with the direct method on the two lenses in presence or absence of SOE and distinguished between those measured at 50% efficiency and those measured at 90% of 0° efficiency, are reported in Tab. 2.

Table 2. Summary of experimental acceptance angles obtained with the direct method

Lens		Prismatic		Hybrid	
SOE		No	Yes	No	Yes
Cell	50%	1.3	1.6	1.2	1.6
	90%	0.5	0.6	0.5	0,6
Sph.	50%	1.4	2.0	1.4	2.0
	90%	0.7	0.7	0.7	0.8

The experimental error has been calculated with the propagation method and is equal to ±0,1° for all the reported angles. We now discuss the experimental results obtained applying the inverse method to both lenses with SOE, as this configuration has given the best results in terms of optical efficiency (higher acceptance angles) and is that used in practice in the C-Modules of PhoCUS system. The first experiments were carried out at a lens-screen distance of d = 3.8m as this was the maximum available space in laboratory. Afterwards, this distance was doubled by placing a mirror between the concentrator and the screen, reaching in this way

a distance d = 7.5m. Fig. 28 shows the optical efficiency profiles obtained for the prismatic lens coupled to the SOE.

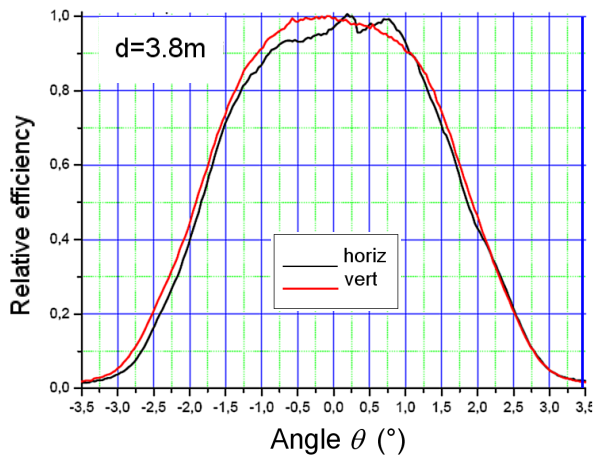

Figure 28. Experimental inverse efficiency curves (vertical and horizontal) of the prismatic lens with SOE at lens-screen distance d = 3.8m

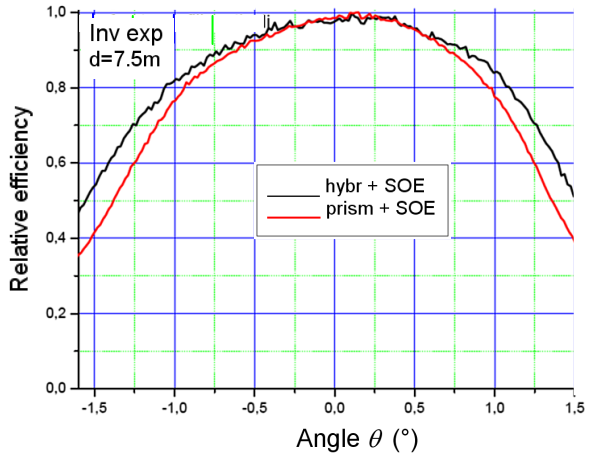

Figure 29. Experimental efficiency of the two lenses with SOE obtained with inverse method at d=7.5m

The angular resolution of the image was in this way reduced to 0.6°. Fig. 29 shows the optical efficiency profile as obtained for the two lenses coupled to the SOE by the inverse method applied at d = 7.5m. The increase of the distance d has now produced the reduction, from about 3.0° to 1.5°, of the maximum angle detectable on the screen by the CCD. Comparing Figs. 28 and 29 it can be seen that the increase of distance d has determined a decrease of acceptance angle for the prismatic lens (in particular from ≈1.8° to ≈1.4° at 50% of 0° efficiency). A summary of the experimental acceptance angles, measured with the inverse method on the two lenses in presence of SOE and distinguishing between those measured at 50% efficiency and those measured at 90% of 0° efficiency, are reported in Tab. 3. The experimental data of optical efficiency discussed so far have been obtained at Ferrara University by indoor measurements. The experiments performed at ENEA Portici were carried out on a similar Mock-up both indoors and outdoors. The results are reported in Tab. 4 and Fig. 30 and can be considered valid for both the prismatic and the hybrid lens [8, 9].

Table 3. Summary of experimental acceptance angles obtained with the inverse method

d(m)	Prismatic		Hybrid	
	50%	90%	50%	90%
3.8	1.9	1.0	2.4	1.4
7.5	1.4	0.7	1.5	0.8

Table 4. Summary of indoor and outdoor data of acceptance angle obtained at ENEA Portici with the direct method

	Indoor		Outdoor	
	50%	90%	50%	90%
No SOE	1.2	0.5	-	0.4
SOE	2.6	0.8	-	0.85

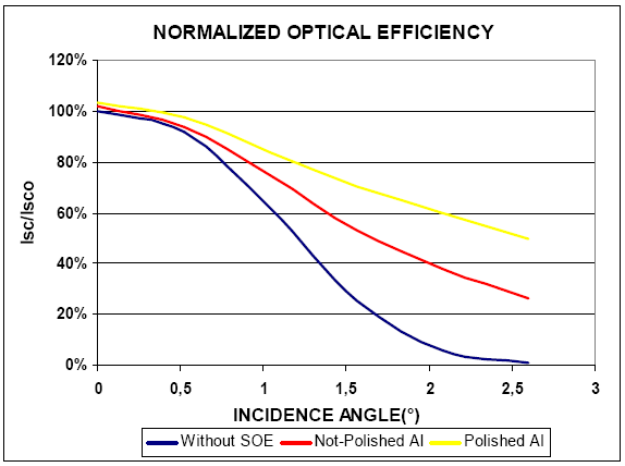

a)

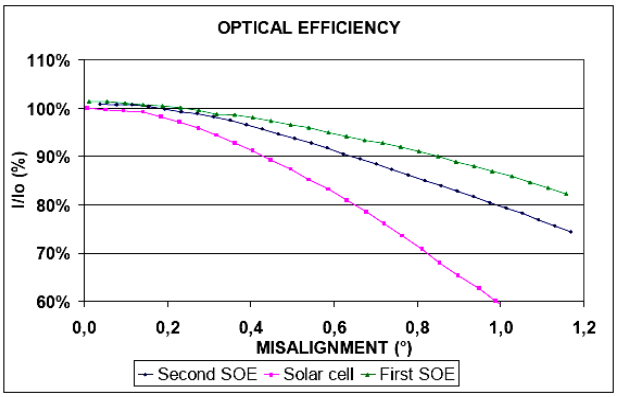

b)

Figure 30. Normalized optical efficiency for three different configurations: a) indoor test; b) outdoor test

The last analysis was the measure of the absolute on-axis (0°) optical efficiency of the Mock-up. The results were: 0.89 ± 0.01 for the prismatic lens and 0.90 ± 0.01 for the hybrid lens.

6. Conclusions

The optical simulations and experiments carried out on the PhoCUS C-Module following both direct and inverse methods allowed to obtain the angle-resolved optical efficiency and the acceptance angles at different operating conditions for both the prismatic and the hybrid lenses. The presence of the secondary optical element (SOE) was essential to reach acceptance angles as high as 0.8° at 90% of 0° efficiency. The on-axis optical transmission was ≈0.9 for both lenses.

Further considerations are to be dedicated to the methods of optical characterization. We have used both the direct and the inverse method, following a simulated or experimental procedure. In all the cases the two methods agree. However, it must be considered that the application of inverse method presents a number of significant advantages, both as regards the duration of the measures and as regards the complexity of the equipment used. In all cases the inverse method is preferable, both for the measurement of the normalized efficiency and for the calculation of the on-axis efficiency.

Appendix

When the inverse method is simulated, the planar screen is configured as an ideal absorber and the measured incident irradiance $E(\theta,\varphi)$ (see Fig. A1a) is converted into the radiance distribution function of the concentrator, $L_{inv}(\theta,\varphi)$, by the $(\cos\theta)^{-4}$ factor. Indeed, if $P(\theta,\varphi)$ is a point on the screen, $E(\theta,\varphi)$ the corresponding incident irradiance and dS an elementary area around $P(\theta,\varphi)$, the flux through area dS is $d\Phi = E(\theta,\varphi)\cdot dS$ and it is confined within the solid angle $d\Omega$ given by:

$$d\Omega = \frac{dS\cdot\cos\theta}{r^2(\theta)} = \frac{dS\cdot\cos\theta}{(d/\cos\theta)^2} = \frac{dS}{d^2}\cdot\cos^3\theta \qquad \text{(A1)}$$

The inverse radiance produced by the concentrator towards (θ,φ) direction will be therefore expressed by:

$$L_{inv}(\theta,\varphi) = \frac{d\Phi}{d\Omega\cdot A_{in}\cdot\cos\theta} = \ldots$$
$$\ldots\frac{E(\theta,\varphi)\cdot dS}{(dS\cdot\cos^3\theta/d^2)\cdot A_{in}\cdot\cos\theta} = \frac{d^2}{A_{in}}\cdot\frac{E(\theta,\varphi)}{\cos^4\theta} \qquad \text{(A2)}$$

where A_{in} is the input aperture area of concentrator. The radiance can be normalized to the value at $\theta = 0°$ giving:

$$L_{inv}^{rel}(\theta,\varphi) = \frac{L_{inv}(\theta,\varphi)}{L_{inv}(0)} = \frac{E(\theta,\varphi)}{E(0)\cdot\cos^4\theta} = \frac{E^{rel}(\theta,\varphi)}{\cos^4\theta} \qquad \text{(A3)}$$

The inverse radiance is related to the optical efficiency of the concentrator in the following way:

$$L_{inv}^{rel}(\theta,\varphi) = \frac{L_{inv}(\theta,\varphi)}{L_{inv}(0)} = \eta_{dir}^{rel}(\theta,\varphi) = \frac{\eta_{dir}(\theta,\varphi)}{\eta_{dir}(0)} \qquad \text{(A4)}$$

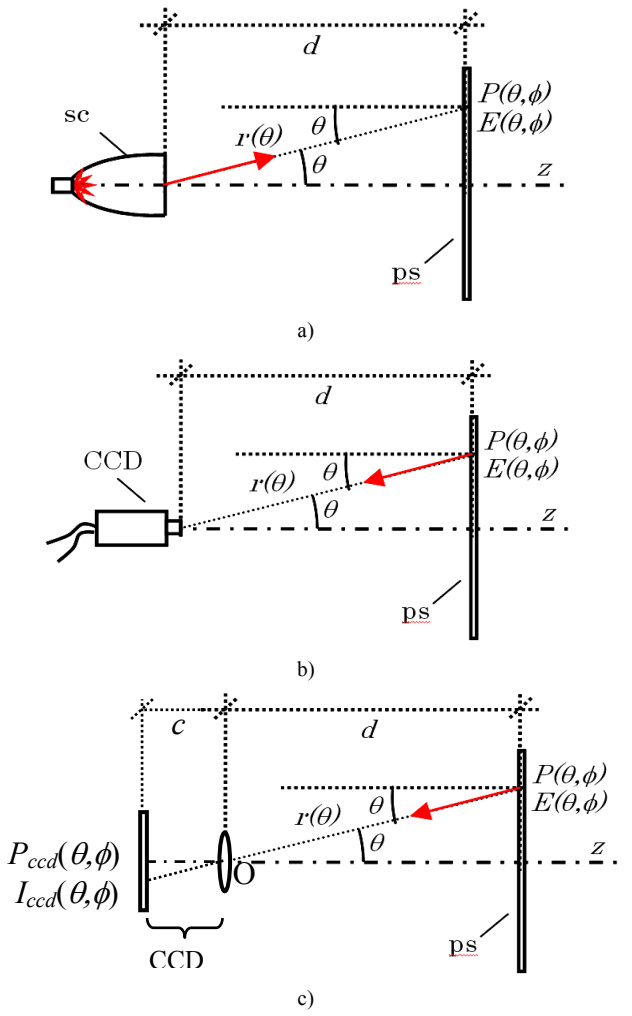

Figure A1. (a) Schematic of the irradiation of the planar screen (ps) by the inverse light produced by the solar concentrator (sc). (b) Process of recording by the CCD of the image produced by the irradiance map produced on the planar screen. $P(\theta,\varphi)$ is a point on the screen and $E(\theta,\varphi)$ is the corresponding incident irradiance. (c) The CCD is schematised as a lens and a plane representing the image sensor of the CCD; $P_{ccd}(\theta,\varphi)$ is a point and $I_{ccd}(\theta,\varphi)$ is the intensity (irradiance) on the CCD sensor

We conclude that, when we simulate the inverse method, the normalized profile of the direct transmission efficiency of the concentrator is directly derived by the normalized irradiance incident on the ideal absorbing screen, by the expression:

$$\eta_{dir}^{rel}(\theta,\varphi) = E^{rel}(\theta,\varphi)\cdot\cos^{-4}\theta \qquad \text{(A5)}$$

When the "inverse" method is applied experimentally, the screen is used to send back the diffuse, inverse light towards the CCD and must have a Lambertian character (reflectivity independent on the incidence angle, and constant radiance of the reflected light, as function of observation angle) in order to allow the reconstruction of the irradiance map on the screen from the intensity map produced on the CCD. If the CCD is aligned with the optical z axis and close to the concentrator (see Fig. A1b), the intensity profile of CCD

image must be corrected by a further $(\cos\theta)^{-4}$ factor, as we demonstrate in the following (see Fig. A1c).

The total flux reflected by the unitary area of (ps) centered in $P(\theta,\varphi)$ is:

$$E_R(\theta,\varphi) = \pi \cdot L_R(\theta,\varphi) \quad \text{(A6)}$$

where R is the reflectance of (ps), $E_R(\theta,\varphi) = R \cdot E(\theta,\varphi)$ is the reflected irradiance, and $L_R(\theta,\varphi)$ is the radiance of the screen. The flux reflected by the unitary area of (ps) and flowing inside the solid angle by which the unitary area is seen by point $O(\theta,\varphi)$ is:

$$\Delta\Phi_R(\theta,\varphi) = L_R(\theta,\varphi) \cdot \frac{\cos^4\theta}{d^2} \quad \text{(A7)}$$

This flux is the same reaching the CCD sensor area $(c/d)^2$ centered on point $P_{ccd}(\theta,\varphi)$. The intensity of the CCD image at point $P_{ccd}(\theta,\varphi)$, proportional to the irradiance incident at that point, is therefore:

$$I_{ccd}(\theta,\varphi) = k \cdot \frac{\Delta\Phi_R(\theta,\varphi)}{(c/d)^2} = \ldots$$

$$k \cdot L_R(\theta,\varphi) \cdot \frac{\cos^4\theta}{c^2} = k \cdot E_R(\theta,\varphi) \cdot \frac{\cos^4\theta}{\pi \cdot c^2} = \ldots \quad \text{(A8)}$$

$$k \cdot R \cdot E(\theta,\varphi) \cdot \frac{\cos^4\theta}{\pi \cdot c^2}$$

By using Eq. (A2), we obtain:

$$I_{ccd}(\theta,\varphi) = \frac{k \cdot R \cdot A_{in}}{\pi \cdot c^2 \cdot d^2} \cdot L_{inv}(\theta,\varphi) \cdot \cos^8\theta \quad \text{(A9)}$$

From Eq. (A9) we finally obtain the inverse radiance of the concentrator from the intensity on the CCD:

$$L_{inv}(\theta,\varphi) = \frac{\pi \cdot c^2 \cdot d^2}{k \cdot R \cdot A_{in}} \cdot I_{ccd}(\theta,\varphi) \cdot \cos^{-8}\theta \quad \text{(A10)}$$

The normalized radiance becomes:

$$L_{inv}^{rel}(\theta,\varphi) = I_{ccd}^{rel}(\theta,\varphi) \cdot \cos^{-8}\theta \quad \text{(A11)}$$

Finally, from Eq. (A4) we obtain the normalized transmission efficiency of the concentrator:

$$\eta_{inv}^{rel}(\theta,\varphi) = I_{ccd}^{rel}(\theta,\varphi) \cdot \cos^{-8}\theta \quad \text{(A12)}$$

REFERENCES

[1] F. Apicella, C. Cancro, P. Ciani, G. Flaminio, G. Graditi, G. Leanza, A. Merola, F. Pascarella, A. Romano, F. Roca, "Development and performance analysis of the PhoCUS C-Module", Proc. 23rd EPSEC, Valencia, Spain, 1-5 September 2008.

[2] A. Sarno, F. Apicella, M. Pellegrino, C. Privato, F. Roca, "Enea experience on the Pv concentrators technology: the Phocus project", Proc. of the 4th International Conference on Solar Concentrators for the Generation of Electricity or Hydrogen, Madrid, Spain, 12-16 March 2007, p. 233-236.

[3] A. Sarno, F. Apicella, M. Pellegrino, C. Privato, F. Roca, "Assessement of Phocus/PV-C Technolgy: technical features and economical aspects", Proc. of the 21st EPSEC, Dresden, Germany, 4-8 September 2006.

[4] A. Parretta, A. Antonini, E. Milan, M. Stefancich, G. Martinelli, M. Armani, "Optical efficiency of solar concentrators by a reverse optical path method", Optics Letters 33 (2008) 2044-2046.

[5] G. Graditi, C. Privato, "La concentrazione fotovoltaica e l'attività di ricerca per i componenti fotovoltaici e di sistema", Zero Emission, Fiera di Roma, 10 September 2010.

[6] E. Bobeico, L. Lancellotti, P. Morvillo, F. Roca, "Metal grid optimization of cSi Solar cells for concentrating systems", Proc. 21st EPSEC, Dresden, Germany, 4-8 September 2006, p. 509-512.

[7] A. Mittiga, "Concentratore rifrattivo a prismi per luce solare", Patent It. n. RM2002A000437.

[8] C. Cancro, G. Graditi, A. Romano, R. Fucci, "Improvements in the PhoCUS C-Module optical devices", Proc. of the 22nd EPSEC, 3-7 September 2007, Milan, Italy, p.731-734.

[9] C. Cancro, R. Fucci, G. Graditi, A. Romano, A. Antonini, M. Armani, "Comparison between two different SOE geometrical shapes to increase the PhoCUS C-Module energy performances", Proc. of the 21st EPSEC, Dresden, Germany, 4-8 September 2006.

[10] E. Bobeico, C. Cancro, R. Fucci, G. Graditi, A. Romano, A. Parretta, A. Antonini, M. Armani, "Elemento Ottico Secondario nel C-Module PhoCUS: progettazione ed analisi delle prestazioni", Class.ne ENE: EGE 05029, 18 Ottobre 2005.

[11] A. Parretta, A. Antonini, "Optics of Solar Concentrators. Part II: Models of light collection of 3D-CPCs under direct and collimated beams", Int. J. of Optics and Applications, 3(5), 2013, 72-102.

[12] A. Parretta, "Optics of Solar Concentrators. Part I: Theoretical models of light collection", Int. J. of Optics and Applications, 3(4), 2013, 27-39.

[13] A. Parretta, L. Zampierolo, A. Antonini, E. Milan, D. Roncati, "Theory of "inverse Method" Applied to Characterization of Solar Concentrators", Proc. 25th EPSEC, Valencia, Spain, 6-10 September 2010.

[14] A. Parretta, D. Roncati, "Theory of the "Inverse Method" for Characterization of Solar Concentrators", Proc. of "Optics for Solar Energy (SOLAR)", Tucson, AZ, USA, 7-10 June 2010, StuE2.

[15] A. Parretta, G. Martinelli, A. Antonini, D. Vincenzi, C. Privato, "Direct and inverse methods of characterization of solar concentrators", Proc. of "Optics for Solar Energy (SOLAR)", Tucson, AZ, USA, 7-10 June 2010, StuA1.

[16] A. Parretta, L. Zampierolo, D. Roncati, "Theoretical aspects of light collection in solar concentrators ", Proc. of "Optics for Solar Energy (SOLAR)", Tucson, AZ, USA, 7-10 June 2010, StuE1.

[17] A. Parretta, A. Antonini, M.A. Butturi, P. Di Benedetto, D. Uderzo, P. Zurru, "Optical Methods for Indoor Characterization of Small-Size Solar Concentrators Prototypes", CIMTEC 2010, 5th Forum on New Materials, Montecatini Terme, Tuscany, Italy, 13-18 June 2010.

[18] A. Parretta, A. Antonini, E. Bonfiglioli, M. Campa, D. Vincenti, G. Martinelli, "Il metodo inverso svela le proprietà dei concentratori solari", PV Technology, n. 3, 2009, pp. 58-64.

[19] A. Parretta, A. Antonini, M.A. Butturi, P. Di Benedetto, E. Milan, M. Stefancich, D. Uderzo, P. Zurru, D. Roncati, G. Martinelli, M. Armani, "How to "Display" the Angle-Resolved Transmission Efficiency of a Solar Concentrator Reversing the Light Path", Proc. 23rd EPSEC, Valencia, Spain, 1-5 September 2008.

[20] A. Parretta, A. Antonini, M. Stefancich, G. Martinelli, M. Armani, "Inverse illumination method for characterization o CPC concentrators", SPIE Optics and Photonics Conf., San Diego, California (USA), 26-30 August 2007.

[21] A. Parretta, A. Antonini, M. Stefancich, G. Martinelli, M. Armani, "Optical Characterization of CPC Concentrator by an Inverse Illumination Method", 22nd European Photovoltaic Solar Energy Conference and Exhibition, Fiera Milano, 3–7 September 2007, Milan, Italy.

[22] A. Parretta, A. Antonini, M. Butturi, P. Zurru, "Optical simulation of Rondine® solar concentrators by two inverse characterization methods", Journal of Optics, 14 (2012) 125704 (8pp).

[23] A. Parretta, A. Antonini, M. Butturi, P. Zurru, "Optical simulation of PV solar concentrators by two inverse characterization methods", Int. Journal of Optics and Applications, 2 (2012) 62-71.

[24] A. Parretta, C. Privato, G. Nenna, A. Antonini, M. Stefancich, "Monitoring of concentrated radiation beam for photovoltaic and thermal solar energy conversion applications", Applied Optics 45, (2006), 7885-7897.